Pluto's atmosphere from the 29 June 2015 ground-based stellar occultation at the time of the New Horizons flyby[1]

B. Sicardy[1], J. Talbot[2], E. Meza[1], J. I. B. Camargo[3,4], J. Desmars[5], D. Gault[6,7], D. Herald[2,7,8], S. Kerr[2,9], H. Pavlov[7], F. Braga-Ribas[10,3,4], M. Assafin[11], G. Benedetti-Rossi[3], A. Dias-Oliveira[3], A. R. Gomes-Júnior[11], R. Vieira-Martins[3], D. Bérard[1], P. Kervella[1,12], J. Lecacheux[1], E. Lellouch[1], W. Beisker[13], D. Dunham[7], M. Jelínek[14,15], R. Duffard[15], J. L. Ortiz[15], A. J. Castro-Tirado[15,16], R. Cunniffe[15], R. Querel[17], P. C. Yock[18], A. A. Cole[19], A. B. Giles[19], K. M. Hill[19], J. P. Beaulieu[20], M. Harnisch[2,21], R. Jansen[2,21], A. Pennell[2,21], S. Todd[2,21], W. H. Allen[2], P. B. Graham[2,22], B. Loader[7,2], G. McKay[2], J. Milner[2], S. Parker[23], M. A. Barry[2,24], J. Bradshaw[7,25], J. Broughton[2], L. Davis[6], H. Devillepoix[26], J. Drummond[27], L. Field[2], M. Forbes[2,22], D. Giles[6,28], R. Glassey[29], R. Groom[30], D. Hooper[2], R. Horvat[6], G. Hudson[2], R. Idaczyk[2], D. Jenke[31], B. Lade[31], J. Newman[8], P. Nosworthy[6], P. Purcell[8], P. F. Skilton[2,32], M. Streamer[8], M. Unwin[2], H. Watanabe[33], G. L. White[6],

and

D. Watson[2]

bruno.sicardy@obspm.fr

[1]LESIA/Observatoire de Paris, PSL, CNRS UMR 8109, University Pierre et Marie Curie, University Paris-Diderot, 5 place Jules Janssen, F-92195 Meudon Cédex, France

[2]Occultation Section of the Royal Astronomical Society of New Zealand (RASNZ)

[3]Observatório Nacional/MCTI, R. General José Cristino 77, Rio de Janeiro - RJ, 20.921-400, Brazil

[4]Laboratório Interinstitucional de e-Astronomia - LIneA, Rua Gal. José Cristino 77, Rio de Janeiro, RJ 20921-400, Brazil

[5]IMCCE/Observatoire de Paris, 77 Avenue Denfert Rochereau, Paris, F-75014, France

[6]Western Sydney Amateur Astronomy Group (WSAAG), Sydney, NSW, Australia

[7]International Occultation Timing Association (IOTA)

[8]Canberra Astronomical Society, Canberra, ACT, Australia

[9]Astronomical Association of Queensland, QLD, Australia

[10]Federal University of Technology - Paraná (UTFPR/DAFIS), Rua Sete de Setembro, 3165, CEP 80230-901, Curitiba, PR, Brazil

[11]Universidade Federal do Rio de Janeiro, Observatório do Valongo, Ladeira do Pedro Antônio 43, CEP 20080-090, Rio de Janeiro, Brazil

[12]Unidad Mixta Internacional Franco-Chilena de Astronomía (UMI 3386), CNRS/INSU, France & Departamento de Astronomía, Universidad de Chile, Camino El Observatorio 1515, Las Condes, Santiago, Chile

[13]IOTA/ES, Bartold-Knaust-Strasse 8, D-30459 Hannover, Germany

[14]Astronomical Institute of the Czech Academy of Sciences, Fričova 298, CZ-25165 Ondřejov, Czech Republic

[15]Instituto de Astrofísica de Andalucía-CSIC, Aptd 3004, E-18080, Granada, Spain

[16]Departamento de Ingeniería de Sistemas y Automática, E.T.S. de Ingenieros Industriales, Universidad de Málaga, Unidad Asociada al CSIC, Málaga, Spain

[17]National Institute of Water and Atmospheric Research (NIWA), Lauder, New Zealand

Received _____; accepted _____

Submitted to ApJ Letters

[18]Department of Physics, University of Auckland, Private Bag 92019, Auckland, New Zealand

[19]School of Physical Sciences, University of Tasmania, Private Bag 37, Hobart, TAS 7001, Australia

[20]Sorbonne Universités, Université Pierre et Marie Curie et CNRS, UMR 7095, Institut d'Astrophysique de Paris, 98 bis bd Arago, 75014 Paris, France

[21]Dunedin Astronomical Society, Dunedin, New Zealand

[22]Wellington Astronomical Society (WAS), Wellington, New Zealand

[23]Backyard Observatory Supernova Search (BOSS), Australia and New Zealand

[24] Univ. of Sydney, Elect. and Info. Engineering Dpt, Camperdown, 2006 NSW, Australia

[25]Samford Valley Observatory, QLD, Australia

[26]International Centre for Radio Astronomy Research (ICRAR), and the Department of Applied Geology, Curtin University, Bentley, WA 6102, Australia

[27]Possum Observatory, Patutahi, New Zealand

[28]Penrith Observatory, Western Sydney University, Sydney, NSW, Australia

[29]Canterbury Astronomical Society, Christchurch, New Zealand

[30]Astronomical Society of Western Australia, P.O. Box 421, Subiaco, Perth, WA 6904, Australia

[31]Stockport Observatory, Astronomical Society of South Australia, Stockport, SA, Australia

[32]Mornington Peninsula Astronomical Society, Mount Martha, VIC, Australia

[33]Japan Occultation Information Network (JOIN), Japan

ABSTRACT

We present results from a multi-chord Pluto stellar occultation observed on 29 June 2015 from New Zealand and Australia. This occurred only two weeks before the NASA New Horizons flyby of the Pluto system and serves as a useful comparison between ground-based and space results. We find that Pluto's atmosphere is still expanding, with a significant pressure increase of 5±2% since 2013 and a factor of almost three since 1988. This trend rules out, as of today, an atmospheric collapse associated with Pluto's recession from the Sun. A central flash, a rare occurrence, was observed from several sites in New Zealand. The flash shape and amplitude are compatible with a spherical and transparent atmospheric layer of roughly 3 km in thickness whose base lies at about 4 km above Pluto's surface, and where an average thermal gradient of about 5 K km^{-1} prevails. We discuss the possibility that small departures between the observed and modeled flash are caused by local topographic features (mountains) along Pluto's limb that block the stellar light. Finally, using two possible temperature profiles, and extrapolating our pressure profile from our deepest accessible level down to the surface, we obtain a possible range of 11.9-13.7 μbar for the surface pressure.

Subject headings: occultations — Kuiper belt objects: individual (Pluto) — planets and satellites: atmospheres — techniques: photometric

1. Introduction

Ground-based stellar occultations probe Pluto's atmosphere at radii ranging from $r \sim 1190$ km from the planet center (pressure $p \sim 10$ μbar) up to $r \sim 1450$ km ($p \sim 0.1$ μbar). In a previous work (Dias-Oliveira et al. 2015, DO15 hereafter), we analyzed high signal-to-noise-ratio occultations observed in 2012 and 2013, and derived stringent constraints on Pluto's atmospheric profiles (density, pressure and temperature profiles). and on Pluto's radius ($R_P = 1190 \pm 5$ km, assuming no troposphere). We also found a pressure increase of $6 \pm 1\%$ between 2012 and 2013.

Here we analyze a stellar occultation, observed on 29 June 2015 from Australia and New Zealand, which occurred two weeks before the NASA New Horizons (NH hereafter) flyby of the Pluto system. Our goals are: (1) assess further pressure changes between 2013 and 2015 (eventually providing useful constraints on Pluto's seasonal models); (2) analyze the central flash that was detected for the first time ever from multiple stations. It constrains the thermal structure of a layer immediately above Pluto's surface, its possible departure from sphericity and/or presence of hazes; and (3) constrain the pressure at Pluto's surface. Besides serving as a useful comparison with the NH results, our work is one more benchmark in the long-term survey of Pluto's atmosphere over the forthcoming years.

---

[1]Partly based on observations made with the ESO WFI camera at the 2.2 m Telescope (La Silla), under program ID 079.A-9202(A) within the agreement between the ON/MCTI and the Max Planck Society, with the ESO camera NACO at the Very Large Telescope (Paranal), under program ID 089.C-0314(C), and at the Pico dos Dias Observatory/LNA, Brazil.

2. The 29 June 2015 occultation

The prediction procedures are described in DO15, Assafin et al. (2010) and Benedetti-Rossi et al. (2014). The event was monitored from Australia and New Zealand (Table 1), from which we obtained eight occultation detections. The reconstructed occultation geometry is displayed in Fig. 1, see also Table 2. The light-curves were obtained from classical aperture photometry, after correction of low frequency variations (caused by changing sky conditions) by means of nearby reference stars, when available. The resulting light-curves $\phi(t)$ give the total flux from the star and Pluto's system, normalized to unity outside the occultation, as a function of time t (Fig. 2). The observed flux ϕ can be written:

$$\phi = (1 - \phi_P) \cdot F_\star + \phi_P, \tag{1}$$

where $F_\star$ is the (useful) stellar flux alone, normalized between zero and unity. Thus, ϕ_P and $1 - \phi_P$ are the contributions of Pluto's system and the unocculted stellar flux to ϕ, respectively.

The quantity ϕ_P is in principle measured independently when Pluto and the occulted star are angularly resolved, providing $F_\star$. It is difficult in practice and requires high photometric accuracy on the star, Pluto and nearby reference stars hours or days away from the event. During that time, sky and instrument conditions may vary. Moreover, for data taken without a filter (broadband), chromatic dependence of the extinction adds further systematic biases, especially if calibrations are not made at the same airmass.

One station that went deep into Pluto's shadow (BOOTES-3, broadband, Castro-Tirado et al. 2012) obtained calibration images hours before the event, as the star and Pluto were marginally resolved. However, the overlap of the star and Pluto images prevents the useful determination of the Pluto/star ratio at the required accuracy (1% or better). Moreover the airmass variation (1.1 during calibration vs. 1.6 during the occultation)

introduces unmodeled chromatic effects due to color differences between the star and Pluto. More images taken the following night at very high airmass (3.6) do not provide further constraints on ϕ_P.

One light-curve (Dunedin) was affected by non-linearity caused by a so-called "γ factor" (Poynton 1997) that modified the pixel values to increase the image dynamical range . The (supposedly) reverse transformation provides an event that is globally not deep enough considering its duration, indicating residual non-linearities. Thus, for this station, we only used the bottom part of the light-curve (Fig. 2), assuming that in this range, the retrieved flux ϕ is an affine function of the stellar flux, $\phi = a \cdot F_\star + b$.

In spite of the lack of accurate measurements for ϕ_P, the amplifying effect of the central flash still constrains the thermal structure of Pluto's deepest atmospheric layers (see Section 4).

3. Pressure evolution

The DO15 model uses the simplest possible hypotheses, i.e. Pluto's atmosphere (1) is pure nitrogen (N_2), (2) is spherically symmetric, (3) has a time-independent thermal structure, derived itself from the light-curves, and (4) is transparent (haze-free). The validity of hypotheses (1)-(3) is discussed in DO15. Hypothesis (4) is discussed later in view of the NH results. Adjusting the pressure p_0 at a reference radius r_0 (for a given event) uniquely defines the molecular density profile $n(r)$, from which synthetic light-curves are generated and compared to the data. Note that p_0 monitors the evolution of Pluto's atmospheric pressure as a whole. In practice, most of the contribution to the fits comes from the half-light level ($F_\star \sim 0.5$, $r \sim 1295$ km, $p \sim 1.7$ μbar), with a tapering off above $r \sim 1450$ km ($F_\star \sim 0.9$, $p \sim 0.1$ μbar) and below $r \sim 1205$ km ($F_\star \sim 0.1$, $p \sim 8$ μbar).

The parameters of our model are listed in Table 2 and our simultaneous fits are displayed in Fig. 2. They have χ^2 per degree of freedom close to unity, indicating satisfactory fits. Two minor modifications were introduced, relative to the DO15 model. First, we updated for consistency Pluto's mass factor to $GM = 8.696 \times 10^{11}$ m^3 s^{-2} (Stern et al. 2015), instead of 8.703×10^{11} m^3 s^{-2}, causing negligible changes at our accuracy level. Second, we use the NH-derived Pluto radius ($R_P = 1187$ km) as a boundary condition for the DO15 model. This new value modifies (at a few percent level) the retrieved pressure at a given radius compared to DO15. Moreover, changing R_P translates vertically all the profiles near the surface by an equivalent amount. In other words, all the quantities of interest (pressure, density, temperature) are well defined in terms of altitude above the surface, if not in absolute radius.

The pressures p_0 at $r_0 = 1215$ km and 1275 km are given in Table 2. They are useful benchmarks, respectively corresponding to the stratopause (maximum temperature of 110 K), and the half-light level layer. Fig. 3 displays the pressure evolution over 2012-2015. The formal error bars assume an invariant temperature profile, but this assumption should not affect the *relative* pressure changes in 2012-2015. Relaxing that constraint, we can retrieve p_0 by inverting individual light-curves and testing the effects of the inversion parameters. This yields possible biases estimated to $\pm 0.2, \pm 0.8$ and ± 0.5 μbar in 2012, 2013 and 2015, respectively. We have added for comparison occultation results from 1988 (Yelle & Elliot 1997) and 2002 (Sicardy et al. 2003). They stem from different analyses and may also be affected by biases. However, Fig. 3 should capture the main trend of Pluto's atmosphere, i.e. a monotonic increase of pressure since 1988.

4. Central flash

Nearly diametric occultation light-curves (but still avoiding the central flash) have flat bottoms (Fig. 2). Our ray tracing code shows that near the shadow center, the stellar rays come from a "flash layer" about 3 km in thickness just above $r = 1191$ km, thus sitting 4 km on top of the assumed surface ($R_P = 1187$ km, Fig. 3).

Let us denote by F a model for the stellar flux (distinguishing it from the observed flux $F_\star$). Deep inside Pluto's shadow, F is roughly proportional to the local density scale-height, $H_n = -n/(dn/dr) = T/[\mu g/k + (dT/dr)]$, where μ is the molecular weight, g is the acceleration of gravity and k is Boltzmann's constant (DO15). For a spherical atmosphere, we have also $F \propto 1/z$, where z is the distance to the shadow center. Writing $z = \sqrt{\rho^2 + l^2}$, where ρ is the closest approach distance to the shadow center and l is the distance traveled from that point, we obtain:

$$F \propto \frac{H_n}{z} = \frac{T}{\mu g/k + dT/dr} \cdot \left(\frac{1}{\sqrt{\rho^2 + l^2}} \right). \tag{2}$$

For an approximatively pure N_2 atmosphere ($\mu = 4.652 \times 10^{-26}$ kg), we obtain $\mu g/k \sim 2$ K km^{-1}. As the thermal gradient dT/dr is several degrees per kilometer at the flash layer (see below), the flash amplitude is significantly controlled by dT/dr.

Our best model minimizes $\chi^2 = \sum_i \left\{ \phi_i - \left[(1 - \phi_P)\, F_i + \phi_P \right] \right\}^2 / \sigma_i^2$, where σ_i^2 is the variance of ϕ_i associated with the noise for the $i^{\rm th}$ data point. As we do not measure ϕ_P, we considered it as a free, adjustable parameter. Among the data sets analyzed by DO15, only one had sufficient quality - from the 18 July 2012 ESO Very Large Telescope - to permit a measurement of ϕ_P and thus constrain dT/dr in the deepest accessible layer. It showed that the residual stellar flux, $F_{\rm res}$, at the bottom part of the light-curve lay in the range 0.010-0.031, thus imposing a thermal gradient near the surface (and imposing ϕ_P for the other light-curves). Since $F_{\rm res}$ was determined to within a factor of three, a large

error bar on dT/dr deep in Pluto's atmosphere was obtained, causing difficulties when extrapolating the pressure down to the surface. In doing so, we obtained a possible range $p_{\rm surf}$ = 10-12 μbar for the surface pressure in 2012, estimated at $r = 1190 \pm 5$ km.

As F is roughly constant at the bottom of occultation light-curves (far from the flash), there is a degeneracy between F and ϕ_P: higher values of ϕ_P can be accommodated by smaller values of F, i.e. smaller H_n. This is *not* true anymore within the flash, as F suffers significant variations. The χ^2-minimization provides both ϕ_P and H_n through $\partial\chi^2/\partial\phi_P = 0$ and $\partial\chi^2/\partial H_n = 0$. Although our ray tracing code generates exact values of F for a given model, it is convenient here (for sake of illustration) to note that F is essentially proportional to H_n (Eq. 2), so that $\partial F/\partial H_n \sim F/H_n$. Detailed calculations show that at minimum χ^2, we have $\partial^2\chi^2/\partial H_n^2 = (2N/H_n^2)(\sigma_F^2/\sigma^2)$ for $F \ll 1$, where $\sigma_F^2 = \overline{F^2} - \overline{F}^2$ is the variance of F (the bars denoting average values) and N is the number of data points. Thus, the relative error bar on the scale-height is $\delta H_n/H_n \sim (\sigma/\sigma_F)/\sqrt{N}$, which is small if the flash (and then σ_F) is large.

Since F increases as H_n increases or ρ decreases, H_n and ρ are correlated. However, the full width at half maximum (FWHM) of the flash is proportional to ρ, while H_n controls homogeneously the flash amplitude, keeping its FWHM constant. This disentangles the effects of H_n and ρ. More importantly, the BOOTES-3 and Dunedin stations exhibit flashes with similar amplitudes (Fig. 2). This robustly forces the two stations to be symmetrically placed with respect to the shadow center (Fig. 1), thus imposing $\rho \approx 45 \pm 2$ km for both stations, independently of H_n (Table 2).

The χ^2-value is minimized for $dT/dr = 8.5 \pm 0.25$ K km^{-1} at 1191 km in our model. This particular value must be considered with caution, as it is not representative of the entire flash layer. Due to the functional dependence of $T(r)$ (a branch of hyperbola, DO15), the gradient dT/dr varies rapidly around 1191 km. The average thermal gradient in the

flash layer is in fact $\sim$5 K km^{-1}, consistent with a previous flash analysis (Olkin et al. 2014). Besides, it is typical of what is expected from the heating by methane (D. Strobel 2015, private communication). Other functional forms of $T(r)$ could be tested, but this remains outside the scope of this paper. We note in passing that our best 2015 fit implies a residual stellar flux $F_{\rm res} = 0.028$ (Fig. 2) that is compatible with the possible range (0.010-0.031) mentioned earlier for 2012.

Our spherical, transparent atmospheric model essentially captures the correct shape and height of the central flash (Fig. 2). A closer examination of that figure reveals a small flux deficit (relative to the model) at the left side of the BOOTES-3 flash. It remains marginal, however, considering the general noise level. This said, it could be caused by an unmodeled departure of the flash layer from sphericity, but this is not anticipated. An atmosphere of radius r rotating at angular velocity ω has an expected oblateness $\epsilon \sim r^3\omega^2/2GM \sim 10^{-4}$ for a rotation period of 6.4 days, $r \sim 1190$ km and Pluto's GM. Such oblateness causes a diamond-shaped caustic (Elliot et al. 1977) with a span of $4\epsilon r <\sim 1$ km in the shadow plane. This is negligible considering the closest approach distances involved here ($\sim$45 km). Moreover, expected zonal winds of less than a few meters per second near 1191 km (Vangvichith 2013; Zalucha & Michaels 2013) would have even smaller effects. More complex distortions may arise, as varying thermal conditions along Pluto's limb may slightly tilt the local iso-density layer, but its modeling remains outside the scope of this paper.

A possible explanation of the small discrepancy is that the primary and/or secondary stellar images hit topographic features while moving around Pluto's limb. Curvature effects strongly stretch the images parallel to the limb during the central flash, by a ratio equal to the flash layer radius (1191 km) divided by the closest approach distance, about 45 km. From the star magnitudes (Table 2 and Kervella et al. 2004), we estimate its

diameter as 33 μas, or 0.76 km projected at Pluto. The length of the stellar image is then $0.76 \times (1191/45) \sim 20$ km. It moves at about 4 km above the surface, which is comparable to the local topographic features reported from NH (Stern et al. 2015). It is thus possible that part of the stellar flux was partially blocked by mountains, causing small observed drop. This can be tested by studying the topography derived from NH, noting that the primary and secondary stellar images at BOOTES-3 probed regions near longitude 190°E and latitude 20°S, and 10°E and 20°N, respectively, during the flash.

Finally, NH images reveal tenuous hazes with normal optical depth $\tau_N \sim 0.004$ and scale-height $H = 50$ km (Stern et al. 2015). This implies an optical depth along the line of sight of $\tau \sim \sqrt{2\pi r/H} \cdot \tau_N \sim 0.05$, which is indistinguishable from the noise level (Fig. 2), supporting our transparent-atmosphere hypothesis.

5. Surface pressure

Fig. 3 displays our best pressure profile, with $p_{1191} = 11.0 \pm 0.2$ μbar at the deepest accessible level. To estimate the surface pressure, we need to extrapolate $p(r)$ into the blind zone. Two possible temperature profiles are considered, beside the DO15 model (Fig. 3). One has a temperature gradient in the blind zone that tends to zero at the surface, where $p_{\rm surf} = 13.0$ μbar and $T_{\rm surf} = 36$ K. This describes a shallow troposphere that is in vapor pressure equilibrium with the surface, an example of a locally sublimating N_2 frost layer. The other profile has a constant gradient of 8.5 K km^{-1}, with $p_{\rm surf} = 12.6$ μbar and $T_{\rm surf} = 49$ K. Such warmer regions are indeed observed on Pluto (Lellouch et al. 2000), and they do not sublimate due to the absence of free N_2 frost. Considering the formal error bar ± 0.2 μbar on p_{1191}, we obtain a range of 12.4-13.2 μbar for the surface pressure under hypotheses (1)-(4) of Section 3, and 11.9-13.7 μbar accounting for the already dicussed possible bias of $\sim \pm 0.5$ μbar. Other thermal profiles should be considered at this point, but

they would not change significantly our result due to the proximity (∼4 km) of our deepest accessible level to the surface, leaving little freedom for $p_{\rm surf}$.

6. Conclusions

The 29 June 2015 stellar occultation provided a snapshot of Pluto's atmosphere, after years of similar observations. Moreover, this was the first event with multi-chord cuts into the central flash. Assuming a spherical and transparent atmosphere as in DO15, we satisfactorily fit all the light-curves, including the central flash part (Fig. 2).

We find that Pluto's atmospheric pressure has been increasing monotonically since 1988, with an augmentation of $5 \pm 2\%$ between 2013 and 2015, and an overall factor of almost three between 1988 and 2015 (Fig. 3). This trend between 1988 and 2013 was confirmed by independent works by Elliot et al. (2003); Pasachoff et al. (2005); Person et al. (2013); Young (2013); Bosh et al. (2015). It is now extended to 2015 and rules out an ongoing atmospheric collapse associated with Pluto's recession from the Sun. This is consistent with high thermal inertia models with a permanent N_2 ice cap over Pluto's north pole, that preclude such collapse (Olkin et al. 2015). Other possible models where N_2 condenses on an unlit cap might announce a pressure decrease in the forthcoming years (Hansen et al. 2015). Further monitoring with occultations and a detailed analysis of the NH data will allow discrimination between those scenarios.

The central flash comes from a ∼3-km-thick layer whose base is 4 km on top of Pluto's surface. The amplitude of the flash is consistent with an average thermal gradient of ~ 5 K km^{-1} in that layer. Small departures from the model might be caused by topographic features along Pluto's limb that block the stellar images.

Extrapolating possible temperature profiles down to the surface, we find a possible

range of 11.9-13.7 μbar for the surface pressure. This is larger than, but compatible with the entry value 11 ± 1 μbar derived from the NH radio occultation experiment (Hinson et al. 2015; Gladstone et al. 2016). At this stage, more detailed investigations of both techniques should be undertaken to see if this difference is significant, or the result of unaccounted effects. In any case, the two techniques validate each other, an excellent prospect for future monitoring of Pluto's atmosphere from ground-based occultations.

We acknowledge support from the French grant "Beyond Neptune II" ANR-11-IS56-0002, and Labex ESEP. The research leading to these results has received funding from the European Research Council under the European Community's H2020 (2014-2020/ERC Grant Agreement 669416 "LUCKY STAR"). EM acknowledges support from the contrato de subvención 205-2014-Fondecyt, Peru. JIBC acknowledges the CNPq/PQ2 fellowship 308489/2013-6. MA acknowledges the FAPERJ grant 111.488/2013, CNPq/PQ2 fellowship 312394/2014-4, and grants 482080/2009-4 and 473002/2013-2. JLO acknowledges funding from Proyecto de Excelencia de la Junta de Andalucía J.A.2012-FQM1776, Spanish grant AYA-2014-56637-C2-1-P, and FEDER funds. AJCT acknowledges support from the Junta de Andalucía (Project P07-TIC-03094) and Univ. of Auckland and NIWA for installing of the Spanish BOOTES-3 station in New Zealand, and support from the Spanish Ministry Projects AYA2012-39727-C03-01 and 2015-71718R Development of the Greenhill Observatory was supported under the Australian Research Council's LIEF funding scheme (project LE110100055). We thank C. Harlingten for the use of the H127 Telescope, and D. and M. Warren for long term support. We thank L. Beauvalet for running the ODIN Pluto's system model, M. W. Buie, S. Gwyn and L. A. Young for providing pre-event Pluto's ephemeris and astrometry, D. P. Hinson and D. F. Strobel for most useful discussions, and the reviewer for useful comments

REFERENCES

Assafin, M., Camargo, J. I. B., Vieira Martins, R., et al. 2010, Astron. Astrophys., 515, A32

Benedetti-Rossi, G., Vieira Martins, R., Camargo, J. I. B., Assafin, M., & Braga-Ribas, F. 2014, Astron. Astrophys., 570, A86

Bosh, A. S., Person, M. J., Levine, S. E., et al. 2015, Icarus, 246, 237

Castro-Tirado, A. J., Jelínek, M., Gorosabel, J., et al. 2012, in Astronomical Society of India Conference Series, Vol. 7, Astronomical Society of India Conference Series, 313–320

Cutri, R. M. 2012, VizieR Online Data Catalog, 2311

Cutri, R. M., Skrutskie, M. F., van Dyk, S., et al. 2003, VizieR Online Data Catalog, 2246

Dias-Oliveira, A., Sicardy, B., Lellouch, E., et al. 2015, ApJ, 811, 53

Elliot, J. L., French, R. G., Dunham, E., et al. 1977, ApJ, 217, 661

Elliot, J. L., Ates, A., Babcock, B. A., et al. 2003, Nature, 424, 165

Gladstone, G. R., Stern, S. A., Ennico, K., et al. 2016, Science, in press

Hansen, C. J., Paige, D. A., & Young, L. A. 2015, Icarus, 246, 183

Hinson, D. P., Linscott, I., Tyler, L., et al. 2015, in AAS/Division for Planetary Sciences Meeting Abstracts, Vol. 47, AAS/Division for Planetary Sciences Meeting Abstracts, #105.01

Kervella, P., Thévenin, F., Di Folco, E., & Ségransan, D. 2004, Astron. Astrophys., 426, 297

Lellouch, E., Laureijs, R., Schmitt, B., et al. 2000, Icarus, 147, 220

Olkin, C. B., Young, L. A., French, R. G., et al. 2014, Icarus, 239, 15

Olkin, C. B., Young, L. A., Borncamp, D., et al. 2015, Icarus, 246, 220

Pasachoff, J. M., Souza, S. P., Babcock, B. A., et al. 2005, Astron. J., 129, 1718

Person, M. J., Dunham, E. W., Bosh, A. S., et al. 2013, Astron. J., 146, 83

Poynton, C. 1997, Chapter 6: Gamma, ed. J. Wiley & Sons, 91

Sicardy, B., Widemann, T., Lellouch, E., et al. 2003, Nature, 424, 168

Stern, S. A., Bagenal, F., Ennico, K., et al. 2015, Science, 350, 292

Tholen, D. J., Buie, M. W., Grundy, W. M., & Elliott, G. T. 2008, Astron. J., 135, 777

Vangvichith, M. 2013, Thèse de Doctorat, Ecole Polytechnique, France

Yelle, R. V., & Elliot, J. L. 1997, Atmospheric Structure and Composition: Pluto and Charon, ed. S. A. Stern & D. J. Tholen, 347

Young, L. A. 2013, Astrophys. J., Lett., 766, L22

Zacharias, N., Finch, C. T., Girard, T. M., et al. 2013, Astron. J., 145, 44

Zalucha, A. M., & Michaels, T. I. 2013, Icarus, 223, 819

Table 1: Circumstances of observations.

Site	Lat. (d:m:s) Lon. (d:m:s) altitude (m)	Telescope Instrument Filter	Exp. Time/ Cycle (s)	Observers remarks
Melbourne Australia	37 50 38.50 S 145 14 24.40 E 110	0.20 m CCD/clear	0.32 0.32	J. Milner occultation detected
Spring Hill Greenhill Obs. Australia	42 25 51.55 S 147 17 15.49 E 650	Harlingten/1.27 m EMCCD/B	0.1 0.1	A. A. Cole, A. B. Giles K. M. Hill occultation detected
Blenheim1 New Zealand	41 32 08.59 S 173 57 25.09 E 18	0.28 m CCD/clear	0.64 0.64	G. McKay occultation detected
Blenheim2 New Zealand	41 29 36.27 S 173 50 20.72 E 38	0.40 m CCD/clear	0.32 0.32	W. H. Allen occultation detected
Martinborough New Zealand	41 14 17.04 S 175 29 01.18 E 73	0.25 m CCD/B	0.16 0.16	P. B. Graham occultation detected
Oxford New Zealand	43 18 36 S 172 13 08 E 66 m	0.35 m CCD/clear	1.28 1.28	S. Parker occultation detected, partially cloudy, not yet analyzed
Darfield New Zealand	43 28 52.90 S 172 06 24.04 E 210	0.25 m CCD/clear	0.32 0.32	B. Loader occultation detected, flash
Christchurch New Zealand	43 31 41 S 172 34 54 E 16	0.15 m CCD/clear	0.25 0.25	R. Glassey occultation detected not yet analyzed
BOOTES-3 station Lauder New Zealand	45 02 17.39 S 169 41 00.88 E 370	Yock-Allen/0.6m EMCCD/clear	0.34368 0.34463	M. Jelínek occultation detected, flash
Dunedin New Zealand	45 54 31. S 170 28 46. E 118	0.35 m CCD/clear	5.12 5.12	A. Pennell, S. Todd M. Harnisch, R. Jansen occultation detected, flash
Glenlee Australia	23:16:09.6 S 150:30:00.8 E 50	0.30 m CCD/clear	0.32 0.32	S. Kerr no occultation detected
Reedy Creek Australia	28 06 29.9 S 153 23 52.0 E 65	0.25 m CCD/clear	0.64 0.64	J. Broughton no occultation detected
Linden Australia	33 42 30.0 S 150 29 43.5 E 583	0.76 m, 0.2 m CCD/clear	0.133, 1.28 0.133, 1.28	D. Gault, R. Horvat L. Davis no occultation detected
Leura Australia	33 43 09.0 S 150 20 53.9 E 903m	0.20 m visual	n.a. n.a.	P. Nosworthy no occultation detected
Penrith Australia	33 45 43.31 S 150 44 30.30 E 96	0.62 m CCD/Clear	0.533 0.533	D. Giles M. A. Barry no occultation detected
St Clair, Australia	33 48 37 S 150 46 37 E 41	0.35 m CCD/Clear	0.04 0.04	H. Pavlov no occultation detected
Murrumbateman Australia	34 57 31.50 S 148 59 54.80 E 594	0.40 m & 0.35 m CCD/clear	0.16 & 2 0.16 & 2	D. Herald, M. Streamer no occultation detected
Nagambie Australia	36 47 05.71 S 145 07 59.14 E 129	0.20 m CCD/clear	0.64 0.64	D. Hooper no occultation detected

Table 2: Input parameters and results

Input parameters			
Star			
Coordinates at epoch (J2000)[1]	α= 19$^{\rm h}$ 00$^{\rm m}$ 49.4801$^{\rm s}$ $\pm$ 11 mas, δ= -20$^{\rm d}$ 41' 40.801"$\pm$17 mas		
B, V, R, K magnitudes[2]	12.8, 12.2, 12.8, 10.6		
Pluto parameters			
Pluto's geocentric distance, shadow velocity[3]	4.77070×10^9 km, 24.1 km s^{-1} (at 16:53 UT)		
Pluto's mass and radius[4] (Stern et al. 2015)	$GM = 8.696 \times 10^{11}$ m^3 s^{-2}, $R_P = 1187$ km		
Sub-observer and sub-solar latitudes[4]	B= +51.66 deg, B'= +51.46 deg		
Pluto's north pole position angle[4]	P= +228.48 deg		
Results			
Thermal profile (input values for the DO15 model)			
r_1, T_1, $dT/dr(r_1)$, r_2, T_2	1191.1 km, 81.7 K, 8.5 K km^{-1}, 1217.3 km, 109.7 K		
r_3, T_3, r_4, T_4	1302.4 km, 95.5 K, 1392.0 km, 80.6 K		
$c1, c2, c3$	$1.42143317 \times 10^{-3}$, $2.52794288 \times 10^{-3}$, $-2.12108557 \times 10^{-6}$		
$c4, c5, c6$	$-4.88273258 \times 10^{-7}$, $-7.04714651 \times 10^{-8}$, -3.3716945×10^{4}		
$c7, c8, c9$	7.7271133×10^{1}, $-5.86944930 \times 10^{-2}$, $1.48175559 \times 10^{-5}$		
Longitudes and latitudes of half-light sub-occultation points[5]			
ingress			
Greenhill (154°E, 06°N, MT), Blenheim (120°E, 28°N, MT), Martinborough (119°E, 28°N, MT)			
Darfield (115°E, 30°N, MT), Bootes-3 (113°E, 31°N, MT), Dunedin (108°E, 32°N, MT)			
egress			
Greenhill (232°E, 37°S, MT), Blenheim (280°E, 35°S, ET), Martinborough (282°E, 34°S, ET)			
Darfield (286°E, 33°S, ET), Bootes-3 (288°E, 33°S, ET), Dunedin (293°E, 31°S, ET)			
Pressure (quoted errors at 1σ level[6])			
	18 July 2012	04 May 2013	29 June 2015
Pressure at 1215 km, p_{1215}	6.07 ± 0.04 μbar	6.61 ± 0.03 μbar	6.94 ± 0.08 μbar
Pressure at 1275 km, p_{1275}	2.09 ± 0.015 μbar	2.27 ± 0.01 μbar	2.39 ± 0.03 μbar
Surface pressure (Fig. 3)			$11.9 - 13.7$ μbar
Astrometry			
Time of closest approach to shadow center (UT)		Closest approach to shadow center	
BOOTES-3: 16$^{\rm h}$ 52$^{\rm m}$ 54.8 $\pm$ 0.1$^{\rm s}$		45.9 $\pm$ 2 km N of shadow center	
Dunedin: 16$^{\rm h}$ 52$^{\rm m}$ 56.0 $\pm$ 0.1$^{\rm s}$		44.6 $\mp$ 2 km S of shadow center	
Geocenter: 16$^{\rm h}$ 55$^{\rm m}$ 04.9 $\pm$ 0.1$^{\rm s}$		3911.5 $\pm$ 2 km N of shadow center	

[1]See title's footnote for information.

[2]Zacharias et al. (2013); Cutri et al. (2003); Cutri (2012).

[3]PLU043/DE433 ephemeris.

[4]Using Pluto's north pole J2000 position: $\alpha_{\rm p}$= 08$^{\rm h}$ 52$^{\rm m}$ 12.94$^{\rm s}$, $\delta_{\rm p}$= -06$^{\rm d}$ 10' 04.8" (Tholen et al. 2008).

[5]MT= morning terminator, ET= evening terminator.

[6]Formal errors. Possible systematic biases are $\pm 0.2, \pm 0.8$ and ± 0.5 μbar in 2012, 2013 and 2015, respectively (Section 3).

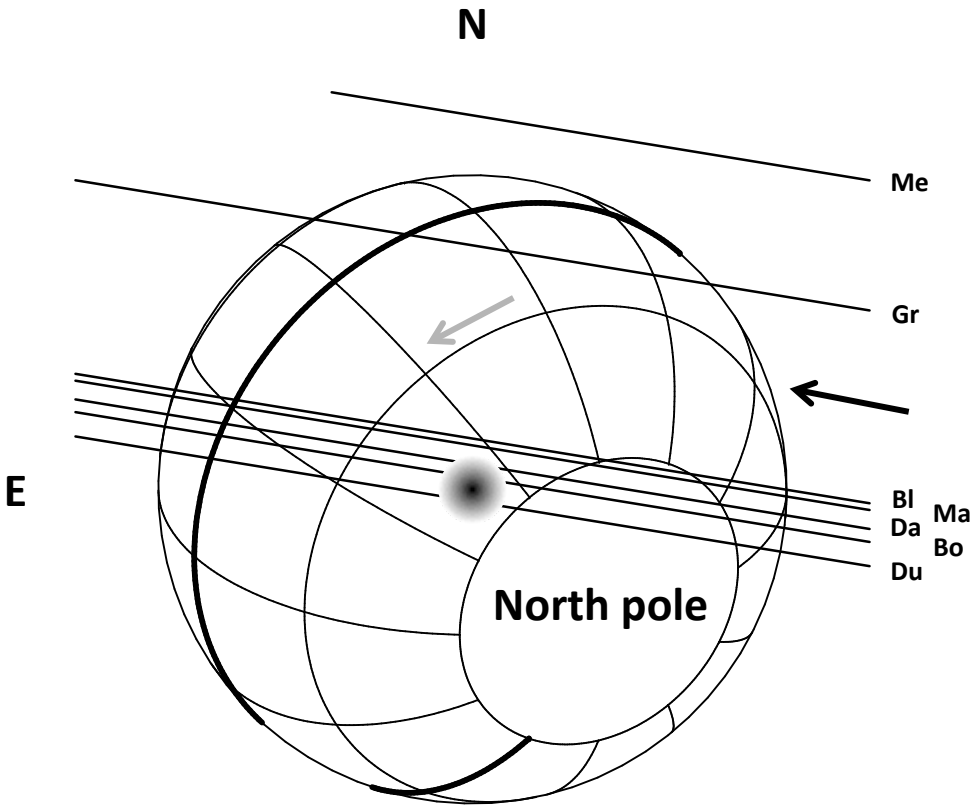

Fig. 1.— Geometry of the 29 June 2015 Pluto stellar occultation. The stellar motion relative to Pluto (black arrow) is shown for seven stations, **Me**: Melbourne, **Gr**: Greenhill, **Bl**: Blenheim, **Ma**: Martinborough, **Da**: Darfield, **Bo**: BOOTES-3, **Du**: Dunedin. The J2000 celestial north and east are indicated by N and E, respectively. Pluto's radius is fixed at 1187 km. The equator and prime meridian are drawn as thicker lines, and direction of rotation is along the gray arrow. The shaded region at center indicates the central flash zone.

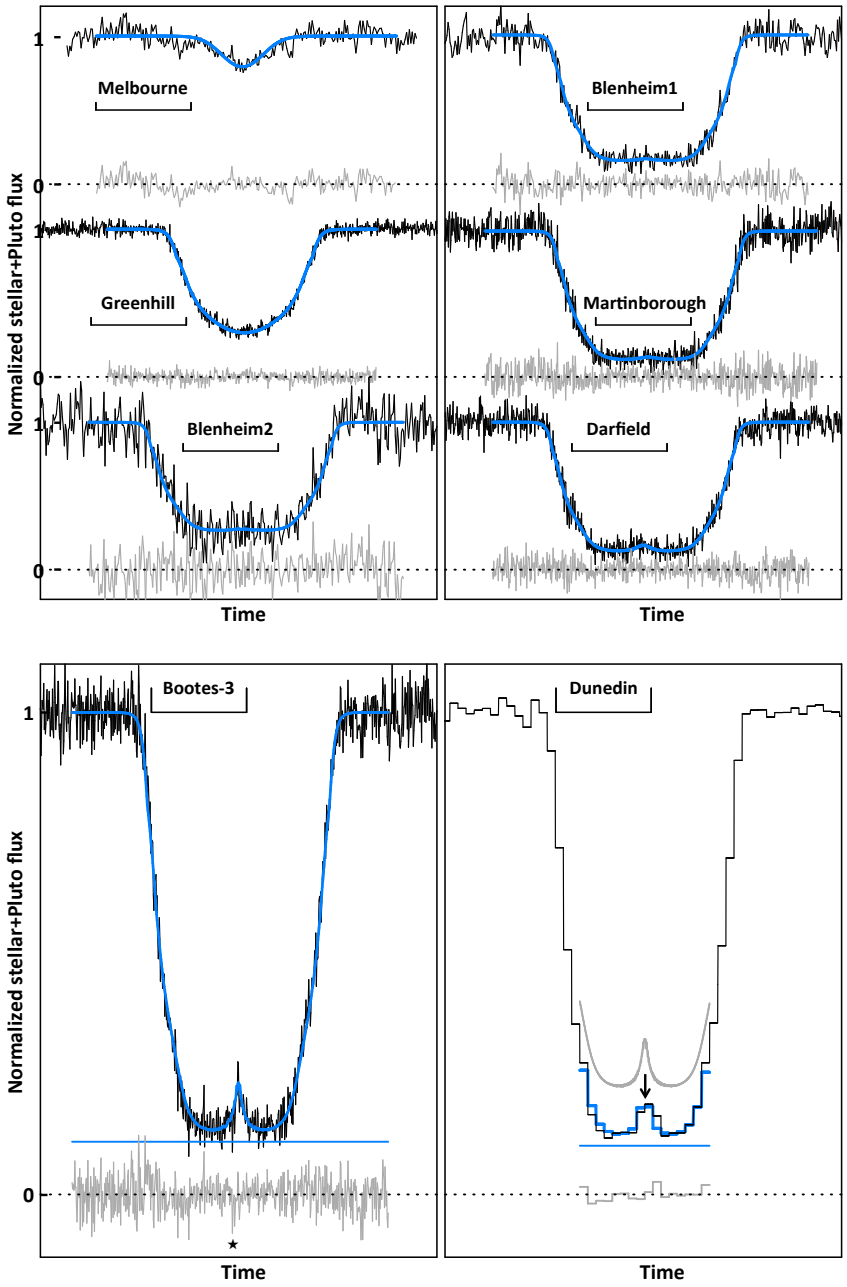

Fig. 2.— Simultaneous fits to our 29 June 2015 occultation light-curves. The intervals under each name correspond to the time-span 16h 52m-16h 43m UT. The model is overplotted in blue, and the residuals are in gray. In the lower panels, the blue horizontal lines are the fitted values of Pluto's contribution to the flux (ϕ_P, Eq. 1). The star symbol under the BOOTES-3 curve indicates a small flux deficit relative to the model. In the Dunedin panel, the smooth curve is the central flash at high resolution, before convolution by the exposure time (5.12 s), vertically shifted for better viewing.

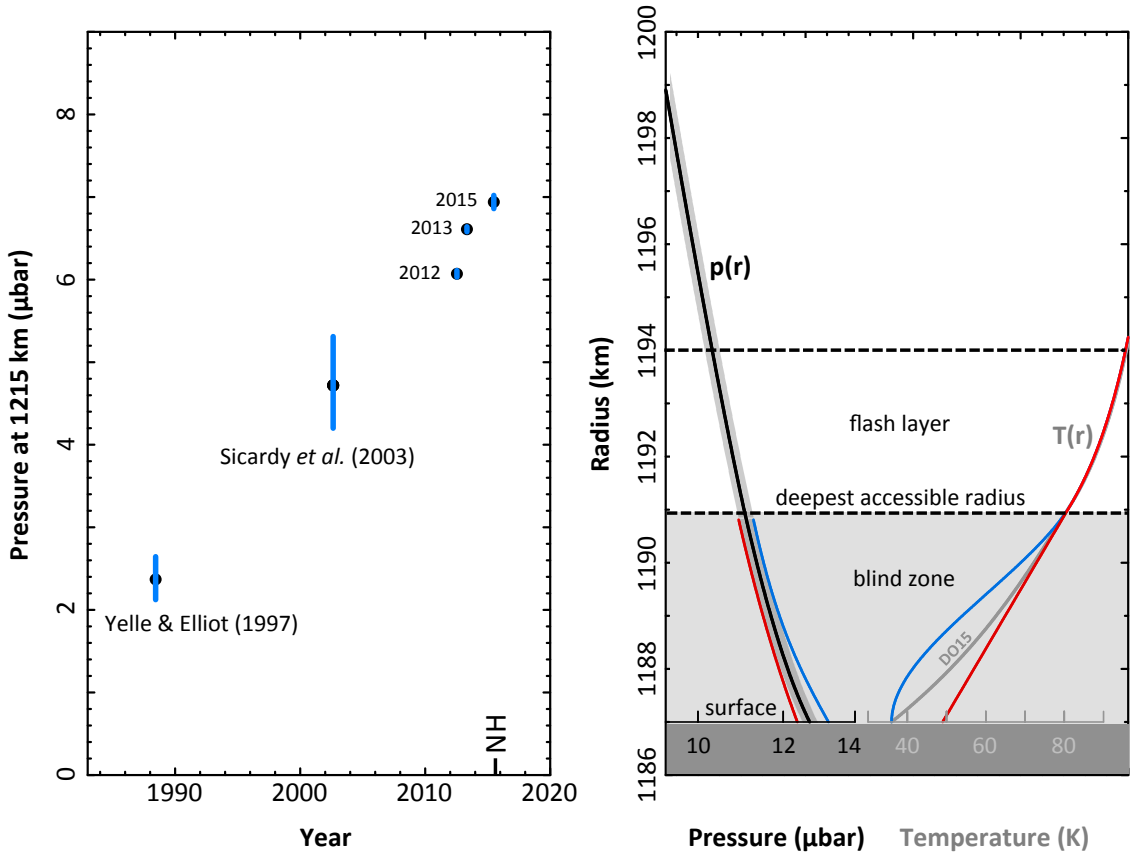

Fig. 3.— Left: Pluto's atmospheric pressure at $r = 1215$ km vs. time in 2012, 2013 and 2015 (our work), and from previous works (Yelle & Elliot 1997; Sicardy et al. 2003), with 1σ error bars. The New Horizons Pluto flyby date (NH) is essentially coincident with our most recent dot. Right: our best pressure profile $p(r)$ for 29 June 2015, with formal 1σ-error domain. The central flash layer roughly lies between the two horizontal dashed lines, above the blind zone below 1191 km. Two possible extrapolations (beside the DO15 model) of temperature profiles $T(r)$ into the blind zone are shown: one with a thermal gradient that reaches zero at the surface (shallow troposphere, blue), and one with a constant gradient 8.5 K km^{-1} (red).